Carbon dots decorated the exposing high-reactive (111) facets CoO octahedrons with enhanced photocatalytic activity and stability for tetracycline degradation under visible light irradiation

Weilong Shi [a,b], Feng Guo [a,c], Huibo Wang [a], Mumei Han [a], Hao Li [a], Songliu Yuan [b], Hui Huang [a,*], Yang Liu [a,*], Zhenhui Kang [a,*]

[a] *Jiangsu Key Laboratory for Carbon-Based Functional Materials & Devices, Institute of Functional Nano & Soft Materials (FUNSOM), Soochow University, 199 Ren'ai Road, Suzhou 215123, Jiangsu, PR China*
[b] *School of Physics, Huazhong University of Science and Technology, Wuhan 430074, PR China*
[c] *Key Laboratory of Subsurface Hydrology and Ecological Effects in Arid Region, Ministry of Education, School of Environmental Science and Engineering, Chang'an University, Xi'an 710064, PR China*

ARTICLE INFO

ABSTRACT

Octahedral CoO with exposed high-reactive (111) facets holds a promising noble-metal-free material in the photocatalysis. However, the (111) facet is usually unstable and easily deactivated during the photocatalytic process as the result of its poloar catastrophe. In this work, carbon dots (CDs) as co-catalyst modified and stabilized the (111) facets of CoO octahedrons (CDs-CoO) were prepared by one-step solvothermal method. The desired CDs-CoO shows the excellent photocatalytic activity and well stability. Meanwhile, the CDs-CoO (5 wt.%) composite exhibits the highest photocatalytic activity for degradation of tetracycline (87%, 60 min), and presents remarkable photostability after five successive cycles (5 h). This enhanced photocatalytic activity and outstanding stability in CDs-CoO composites could be ascribed to several merits of CDs that not only improve charge separation efficiency but also strengthen the interaction between CDs and high-reactive (111) facets of CoO octahedrons.
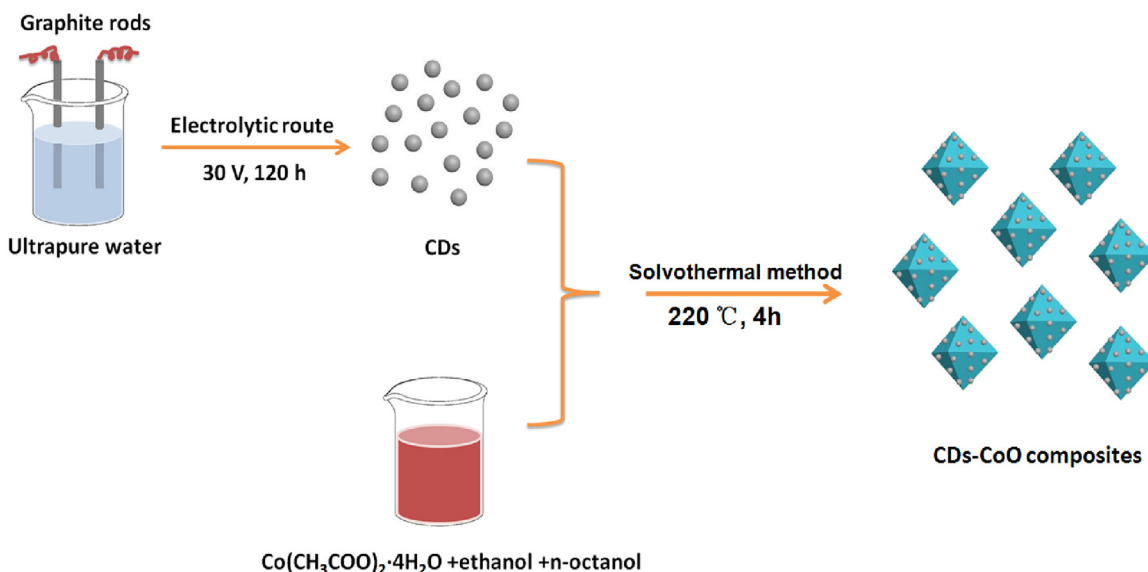
1. Introduction

Semiconductor-based photocatalysis is taken as a promising avenue toward solving current energy and environment problems with abundant solar light, which can mainly be attributed to its less secondary pollution, higher selectivity and lower operating cost [1]. In recent years, the crystal-facet-controlled synthesis of semiconductor photocatalysts has attracted intensive attention in research because their photoelectronic and photocatalytic performances can be further optimized through tailoring the surface atomic structures [2–6]. For instance, the (001) facets of anatase TiO_2 [7], $BiVO_4$ [8], and Bi_2WO_6 [9], Ag_3PO_4 (110) as well as Cu_2O (111) facets [2,10], have been found to contribute significantly for enhancing photocatalytic activities for removal of organic pollutants, water splitting and reduction of CO_2.

Recently, CoO nanostructures possess the enormously potential as a promising photocatalyst, not only with relatively narrow band gap (2.6 eV) for visible light absorption and a solar-to-hydrogen conversion efficiency (~5%), but also with high economic benefit and low productive cost [11]. More recently, CoO octahedrons with exposed high active (111) facets have been fabricated and exhibited excellent photocatalytic activity for degradation of malachite green (MG) under visible light [12]. However, octahedral CoO with the (111) surface facet is quite unstable and easily deactivated due to the fact that Co^{2+} cations and O^{2-} anions alternate from one plane to another, meaning that in the outer surface, these nanostructures have a very polar positive or negative surface of cations or anions, which leads to phase change from CoO to Co_3O_4 for avoiding this polar catastrophe and attaining the thermodynamic stability [13–17]. Thus, it remains an urgent need but a significant challenge to stabilize high active (111) facets of CoO octahedrons and further improve its photocatalytic activity.

Carbon dots (CDs) with sizes below 10 nm, as one of the carbon nanomaterials, have been growing in popularity in a series of areas, such as catalysis [18], sensor [19], bioimaging [20], photovoltaic devices [21], due to its diversely fantastic properties. In particu-

Scheme 1. Schematic illustration of the synthesis procedure to obtain CDs-CoO composite.

lar, CDs possess economies, low-toxicity, robust chemical inertness, easy functionalization, biocompatibility, good water-solubility and photoluminescence (PL) upconversion properties [22–24]. Owing to their outstanding properties, CDs are prone to the modification various organic and inorganic materials to improve the photocatalytic performance and stability, such as CDs/g-C$_3$N$_4$ [25], CDs/TiO$_2$ [23], CDs/Fe$_2$O$_3$ [23], CDs/Ag$_3$PO$_4$ [26], etc. Considering the unstable (111) facets of CoO and the striking advantages of CDs, we attempted to design the composite of decorating CoO octahedrons with CDs (CDs-CoO), and it is expected that this composite may be propitious to enhanced photocatalytic performance and stability. To the best of our knowledge, this is the first report on the investigation of CDs-CoO photocatalyst towards the photocatalytic degradation of organic pollutant.

In the present work, we designed to synthesize CDs (2–8 nm) as co-catalyst anchored on the (111) surface facets of octahedral CoO via one-step solvothermal method for the degradation of tetracycline (TC) under the visible light irradiation. Results show that all the CDs-CoO composites display superior photocatalytic activity than that of the pure CoO, among of which 5% CDs-CoO composite exhibits the highest photocatalytic activity, degrading 87% of TC within 60 min, and presents remarkable photostability after five successive cycles (5 h). This enhanced photocatalytic activity and outstanding stability in CDs-CoO composites can be ascribed to several merits of CDs that not only improve charge separation efficiency but also strengthen the interaction between CDs and high-reactive (111) facets of CoO octahedrons.

2. Experimental section

2.1. Synthesis of CDs-CoO composites

The general process for the fabrication of CDs-CoO is illustrated in Scheme 1. At first, the CDs were prepared through the typical electrochemical method according to our previously report [23]. Subsequently, the prepared CDs solution was treated in a freeze-drying way to obtain the CDs solid powders. Then, CDs/CoO composites with different mass ratios of CDs powders (0 wt.%, 1 wt.%, 3 wt.%, 5 wt.%, 10 wt.% and 20 wt.%) were prepared using the following procedure: 1.84 g Co(CH$_3$COO)$_2$·4H$_2$O and different mass ratios of CDs (0, 0.00552, 0.01656, 0.0276, 0.0552 and 0.1104 g) were added to a mixed solvent containing 64 mL n-octanol and

16 mL ethanol with vigorous stirring for 2 h. The resulted slurry was transferred into a 100 mL Teflon-lined stainless steel autoclave, and then heated at 220 °C for 4 h. The formed powders were washed with ethanol for three times and finally dried at 70 °C in the oven. The CDs/CoO composites with different mass ratios of CDs powders (1 wt.%, 3 wt.%, 5 wt.%, 10 wt.% and 20 wt.%) were abbreviated as 1% CDs-CoO, 3% CDs-CoO, 5% CDs-CoO, 10% CDs-CoO and 20% CDs-CoO, respectively.

2.2. Characterization

Powder X-ray diffraction (XRD) patterns of the samples were recorded using an X'Pert-ProMPD (Holand) D/max-γA X-ray diffractometer with Cu Kα radiation (λ = 0.154178 nm). Transform Infrared (FT-IR) spectrum was characterized by a Nicolet 360 spectrometer. Raman spectra were recorded on an HR 800 Raman spectroscope (JY, France). Scanning electron microscopy (SEM) images and energy dispersive X-ray analysis spectroscopy (EDX) were characterized by an FEI-quanta 200 scanning electron microscope. Transmission electron microscope (TEM), high-resolution TEM (HRTEM) and high-angle annular dark-field scanning transmission electron microscopy (HAADF-STEM) were performed with a FEI-Tecnai F20 microscope operating at 200 kV, respectively. X-ray photoelectron spectroscopy (XPS) was performed on a KRATOS Axis ultra-DLD X-ray photoelectron spectrometer with a monochromatised Al Kα X-ray source. Room temperature UV–vis absorption spectra were recorded on a Lambda 750 (Perking Elmer) spectrophotometer in the wavelength range of 200–800 nm. Photoluminescence (PL) study was recorded on a Fluorolog-TCSPC Luminescence Spectrometer. Electrochemical analysis was conducted on a CHI 660b workstation. The Pt wire, a calomel electrode, and the samples were served as the counter electrode, the reference electrode, and the working electrode in a three-electrode cell. For photocurrent versus time analysis, the 300 W Xe lamp (cutting off λ < 420 nm) and Na$_2$SO$_4$ (0.5 M) was employed as light source and electrolyte. The total organic carbon (TOC) was measured by automatic total organic carbon analyzer (TOC-V, Shimadzu, Japan).

2.3. Photocatalytic activity measurement

Briefly, 50 mg photocatalyst was suspended in 100 mL aqueous solution of 10 mg/L tetracycline (TC). The solution was stirred for
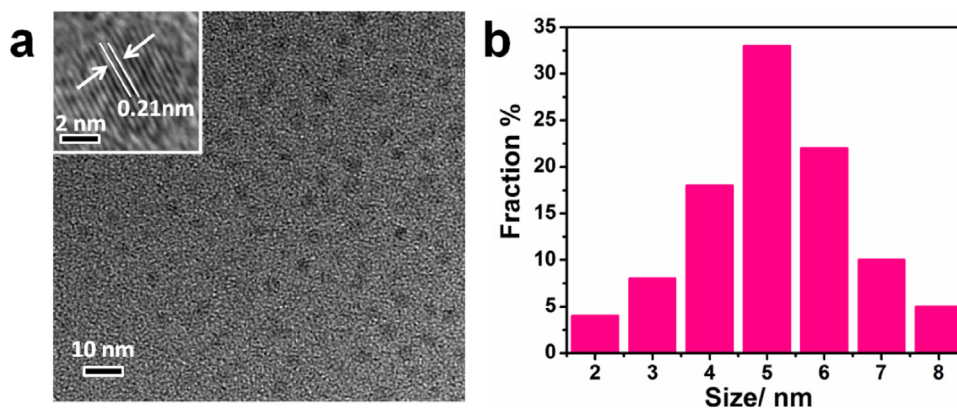
Fig. 1. (a) TEM and HRTEM (inset) images of CDs. (b) The corresponding size distributions of CDs.

30 min in dark to ensure the establishment of adsorption equilibrium. Visible light (300 W, xenon lamp) was obtained by using cut off filters to remove light of $\lambda < 420$ nm. At certain time intervals, 3 mL aliquots were extracted and centrifuged in the reaction process, then analyzed on UV–vis spectrophotometer at the max absorbed wavelength of 357 nm.

2.4. Active species capturing and ESR experiments

Sacrificial agents such as 2-propanol (IPA), disodium ethylenediamine tetraacetic acid (EDTA) and 1,4-benzoquinone (BQ) were used to probe hydroxyl radicals ($^\bullet$OH), holes (h$^+$) and superoxide radicals ($^\bullet$O$_2^-$), respectively. This method was identical with the preceding photocatalytic activity test with the addition of 1 mmol of scavenger. In addition, the electronic spin resonance (ESR) technique was recorded on an electron paramagnetic resonance spectrometer (A300-10/12, Bruker) to further used to detect the presence of $^\bullet$O$_2^-$ radicals in the photocatalytic reaction system under visible light ($\lambda > 420$ nm). The $^\bullet$O$_2^-$ radicals can be captured by the DMPO. Before to determine the superoxide radicals (DMPO-$^\bullet$O$_2^-$), 10 mg samples were dissolved in 0.5 mL methanol (DMPO-$^\bullet$O$_2^-$), and then 45 μL DMPO was added with ultrasonic dispersion for 5 min.

3. Results and discussion

CDs were obtained via an electrochemical method reported according to our previously report. Fig. 1a displays the transmission electron microscopy (TEM) image of CDs, which are well-dispersed and uniform. The high resolution TEM image (HRTEM) image of the individual CDs particle in the inset shows that the crystal lattice spacing is 0.21 nm, agreeing well with the (100) lattice plane of graphitic carbon [27,28]. In addition, we measured around 300 particles, calculating the size distribution of CDs in Fig. 1b, showing that the particle sizes are in the range from 2 to 8 nm, and the average diameter of CDs is about 5 nm.

The XRD patterns of as-synthesized CDs, CoO and CDs-CoO composites are shown in Fig. 2a. All the distinct diffraction peaks in CoO and CDs-CoO composites are corresponded to the face-centered cubic (fcc) structure of CoO (JCPDS 71-1178). However, no characteristic peak for carbon at 26° can be detected in the CDs-CoO composites with the content of CDs from 1 wt.% to 10 wt.%, which may result from the relatively limited CDs amount and low diffraction intensity in the composites [29]. Notably, with the CDs content increasing to 20 wt.% in the composite, an obvious broadened peak at around 26° can be detected, assigning to XRD pattern of CDs. For further insight of possible interactions among CDs-CoO composite, Fourier transform infrared (FT-IR) and Raman spectra analysis were

conducted. Fig. 2b shows the FI-TR spectra of CoO and 5% CDs-CoO to analyze the change in the functional groups. In the FT-IR spectrum of CoO, two main peaks at 420 and 3430 cm^{-1} are attributed to the stretching vibration modes of Co—O and O—H, respectively [30]. For CDs-CoO, the characteristic peaks at C—O—C, C=O and C=C are observed at 1050, 1403 and 1632 cm^{-1}, indicating the existence of CDs in the composite [31]. The Raman spectra ($\lambda_{ex} = 633$ nm) of CoO and CDs-CoO were also recorded and shown in Fig. 2c. For CoO, the absorption bands at 489, 540 and 690 cm^{-1} are identified as E$_g$, T$_{2g}$ and A$_{1g}$ modes of CoO, respectively [32]. While for the CDs-CoO, besides the peaks of CoO, two more characteristic peaks centered at about 1326 and 1602 cm^{-1} are obtained, which can be corresponded to the D-band and G-band of carbon, respectively [33]. Meanwhile, EDX elemental microanalysis from Fig. 2d demonstrates that except for the Si substrate, C, O and Co elements exist in the composite. Based on the above analysis, we can conclude that CoO and CDs-CoO photocatalysts have been successfully synthesized.

The SEM image in Fig. 3a displays the pristine CoO are regular octahedral shape. The exposed facets of these CoO octahedron structures are close to an equilateral triangle, which the edge lengths are in the range of 0.4–1.5 μm and their surfaces are quite smooth, demonstrating strong (111) preferred orientation (inset of Fig. 3a). Significantly, the morphology of 5% CDs-CoO (Fig. 3b) is similar as that of pristine CoO, indicating the loading CDs does not affect the growth of CoO octahedrons. To gain more insight of the 5% CDs-CoO composite, TEM and HRTEM measurements were conducted. The TEM image of 5% CDs-CoO in Fig. 3c shows that CDs are deposited on the surface of octahedral CoO. From the HRTEM image, as displayed in Fig. 3d, a close interface between the CDs and CoO is found in the composite. The lattice spacing of CDs is determined to be 0.21 nm (upper, inset of Fig. 3d), corresponding to the (100) crystal plane of carbon [23], and the lattice spacing around 0.25 nm can be also found (lower, inset of Fig. 3d), which is consistent with the crystallographic (111) spacing of CoO [14]. In addition, the HAADF-STEM images and corresponding elemental mapping images of 5% CDs-CoO were carried out in Fig. 3e, displaying a homogeneous distribution of C, Co and O elements in the CDs-CoO composite.

The surface chemical states of CDs-CoO were investigated by XPS, and the results are given in Fig. 4. The survey spectrum in Fig. 4a shows that the three elements in the sample are Co, O and C. In Fig. 4b, the high-resolution spectrum of C 1 s can be fitted to three peaks locating at 284.5 eV, 285.6 eV and 287.8 eV, assigning to C—C coordination from graphic carbon, C—O and C=O bonds, respectively [34]. For the Co 2p spectrum (Fig. 4c), two separate peaks at 780.7 eV and 796.6 eV with another two relatively obvious satellite peaks at 786.1 and 802.7 eV are obtained, corresponding to
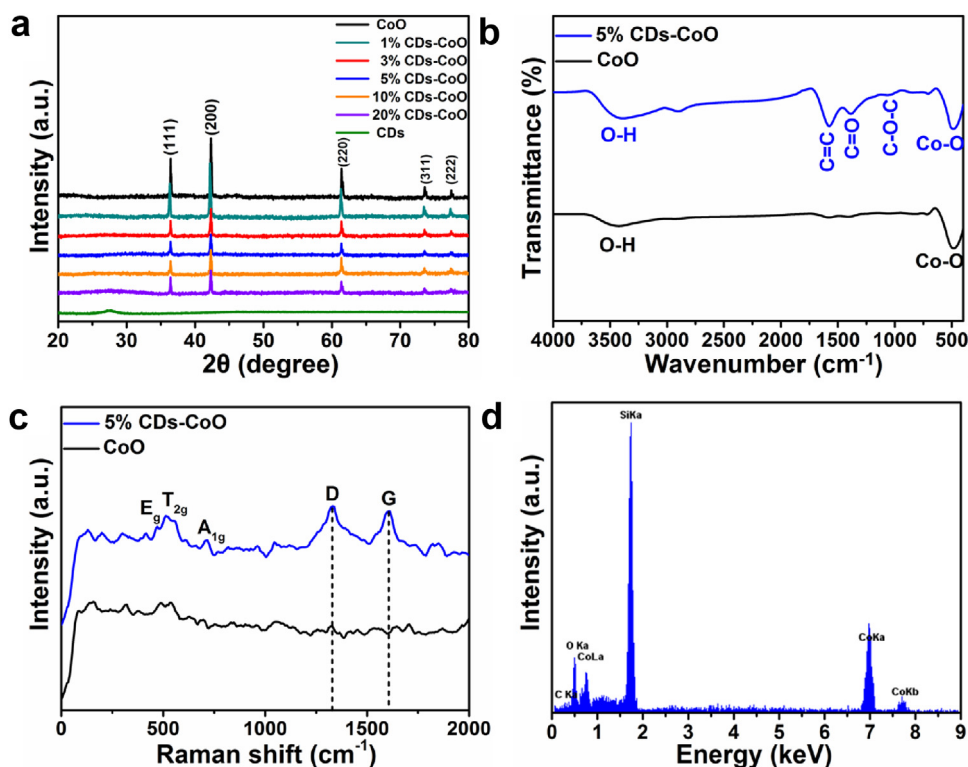
Fig. 2. (a) XRD patterns of as-prepared samples. (b) FT-IR and (c) Raman spectra of CoO and 5% CDs-CoO. (d) EDX elemental microanalysis of 5% CDs-CoO.
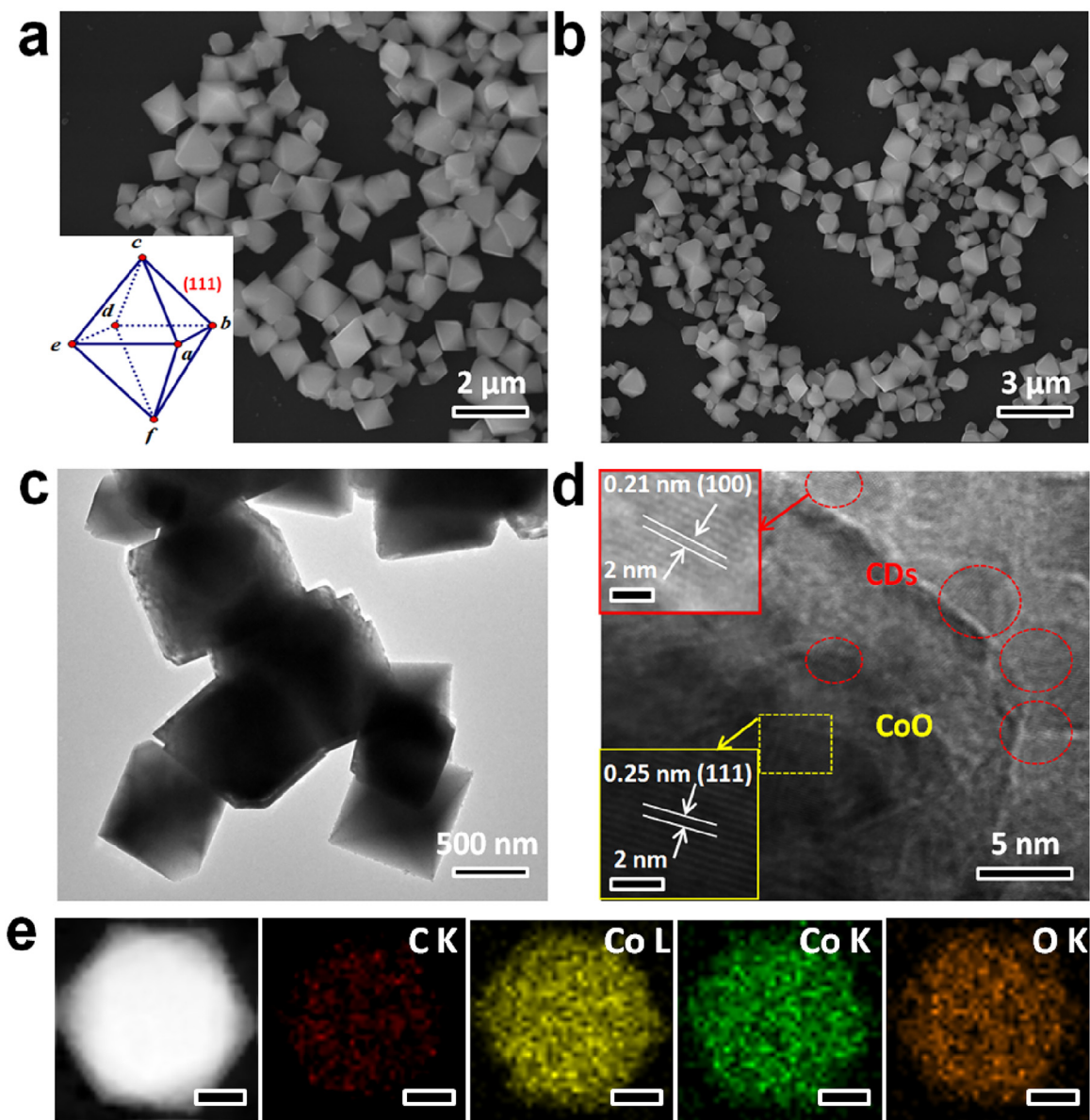
Co $2p_{3/2}$ and Co $2p_{1/2}$ peaks in CoO, respectively [35]. The O 1 s spectrum in Fig. 4d is deconvoluted into four obvious peaks. The binding energy at 529.8 eV is attributed to the Co—O bond [36], while the peak at 531.4 eV is attributed to the Co—O—C bond [37], implying that a strong interaction exists between CDs and CoO. The peaks at around 532.2 eV and 533.5 eV are responsible for the O=C—O and C—OH, respectively [38]. On the basis of XPS findings, it can be concluded that abundant oxygen-containing groups on the surface of CDs can strengthen the interaction between CDs and CoO octahedrons, which may be helpful for stabilizing high active (111) facets of CoO octahedrons.

The optical absorption properties of CoO and 5% CDs-CoO were performed by UV–vis diffuse reflectance spectra. In Fig. 5a, pristine CoO (black trace) exhibits a significant absorption from ultraviolet to visible regions and its band gap absorption edge is around 490 nm. More importantly, after the addition of CDs, 5% CDs-CoO (blue trace) composite presents an obviously enhanced absorption in the visible region, which is beneficial to improving photocatalytic efficiency. Meanwhile, according to the Tauc plot equation [25], the band gap energies of the CoO and 5% CDs-CoO products are estimated to be 2.52 eV and 2.43 eV, respectively (Fig. 5b). To gain a better understanding of energy band structure for 5% CDs-CoO, the Mott-Schottky plot is applied for determining the flat band potential of 5% CDs-CoO. In Fig. 5c, it is obtained that 5% CDs-CoO is a typical p-type semiconductor due to a negative slope [39]. Based on the MS plot, the flat-band potential is determined to be 1.54 V (vs SCE) for the 5% CDs-CoO, which equals to 1.78 V (vs NHE). It is reported that the flat band potential is 0.1–0.3 eV higher than the valence band (VB) in the p-type semiconductor [40,41]. Thus, the VB for 5% CDs-CoO is estimated to be 1.88 V vs. NHE. And the conduction band (CB) position is −0.55 V vs. NHE calculated as based on its band gap. As a result of energy band position, the energy level diagram of 5% CDs-CoO can be obtained and shown in Fig. 5d, implying that as-prepared 5% CDs-CoO composite can produce active specie ($•O_2^-$) for degradation of TC under visible light irradiation in theory.

The photocatalytic performances of as-prepared photocatalysts were measured to degrade TC under visible light irradiation (Fig. 6a). For the blank experiment analysis, the result shows that TC could hardly be degraded after 60 min under visible light irradiation without catalysts, excluding the possibility of self-photolysis in this system. In contrast, the pristine CoO octahedrons exhibit the degradation efficiency of 40% after 60 min visible light irradiation. Significantly, dramatic enhancements in the degradation of TC are obtained with introducing CDs on the surface of CoO octahedrons. Concretely, when increasing the amount of CDs from 1 to 5 wt.%, the degradation of TC increases gradually from 51% to 83% within 60 min under visible light irradiation. However, further increasing the content of CDs over 5 wt.% leads to an evident decrease of degradation performance. This phenomenon that the enhanced photocatalytic activity with the increasing amounts of CDs less than 5 wt.% can ascribe the increasing density of active sites on the surface of octahedral CoO, and the decreased photocatalytic activity with CDs contents exceeded 5 wt.% can result from the shading effect [42]. Fig. 6b shows the changes of two characteristic absorptions of TC under the visible-light irradiation in the present of 5% CDs-CoO as a photocatalyst, proving that the absorption intensities of TC decrease more rapidly with increasing the irradiation time. To quantitatively analyze the catalytic efficiency, the TC degradation rate constants were extracted by assuming pseudo-first-order kinetics (Fig. 6c and d). The results reveal that the photocatalytic behaviors for degradation of TC over as-prepared photocatalysts are well fitted with pseudo-fist-order kinetics. In addition, the 5% CDs content exhibits the highest photodegraded rate constant (0.029 min^{-1}), which is around 4 times larger than the pristine CoO (0.0078 min^{-1}).

In the following experiments, the photocatalytic activity of TC degradation under irradiation using different wavelengths of incident light, TOC removal and cycling tests of 5% CDs-CoO photocatalyst were carried out. Fig. 7a displays the photocatalytic activity of TC degradation concurs with the optical absorption. To

Fig. 3. SEM images of (a) CoO and (b) 5% CDs-CoO composite. (c) TEM and (d) HRTEM images of 5% CDs-CoO composite. (e) HAADF-STEM and the corresponding elemental mapping images of 5% CDs-CoO composite (Scale bar: 200 nm).

determine the mineralization degree of TC during the photocatalytic process, the evolutions of total organic carbon (TOC) over CoO and 5% CDs-CoO were measured. As displayed in Fig. 7b, only 0.4% TOC was removed without photocatalysts, whereas 26.3% and 57.8% TOC removal rates are displayed using CoO and 5% CDs-CoO composite, respectively, which implay the CDs-CoO composites exhibit much higher mineralization efficiency for TC photodegradation. Furthermore, the stability of photocatalysts is essential to the practical applications. Therefore, the cycling runs for the photodegradation of TC with pure CoO and 5% CDs-CoO composite were operated to evaluate its photocatalytic stability (Fig. 7c). In detail, the degradation of TC was evidently decreased over pure CoO, indicating a stepwise deactivation. As a comparison, no obvious deactivation of the CDs-CoO composite is observed and the TC photocatalytic degradation of TC still remains over 75% after five consecutive experiments, which illuminates that the 5% CDs-CoO composite is quite stable during the photocatalytic reaction. Fig. 7d shows that XRD patterns of 5% CDs-CoO before and after photocatalytic reactions have no evident changes. According to the

above analysis, the CDs-CoO composite presents the outstanding photocatalytic activity and stability.

In order to explore the reason of enhanced photocatalytic activity of CDs-CoO, PL and time-resolved fluorescence decay measurements were performed. Fig. 8a shows the PL spectra of CoO and 5% CDs-CoO at the wavelength of 325 nm. It can be seen that 5% CDs-CoO exhibits obviously weaker PL emission peak centered at around 480 nm compared with CoO, indicating that the recombination of photo-generated electron-hole pairs can be effectively hampered and further improving the photocatalytic activity in CDs-CoO composite photocatalytic system. To further understand of the dynamic electron migration process, the time-resolved fluorescence decay spectra of CoO and 5% CDs-CoO were measured and shown in Fig. 8b. As can be seen, the lifetime of CoO and 5% CDs-CoO were 0.51 and 0.62 ns, respectively. The prolonged lifetime of excitons indicates an accelerated charge transfer mechanism induced in the CDs-CoO composite, which is consistent with other previous reports [43–45]. Meanwhile, transient photocurrent responses and EIS experiments were investigated for further confirming the
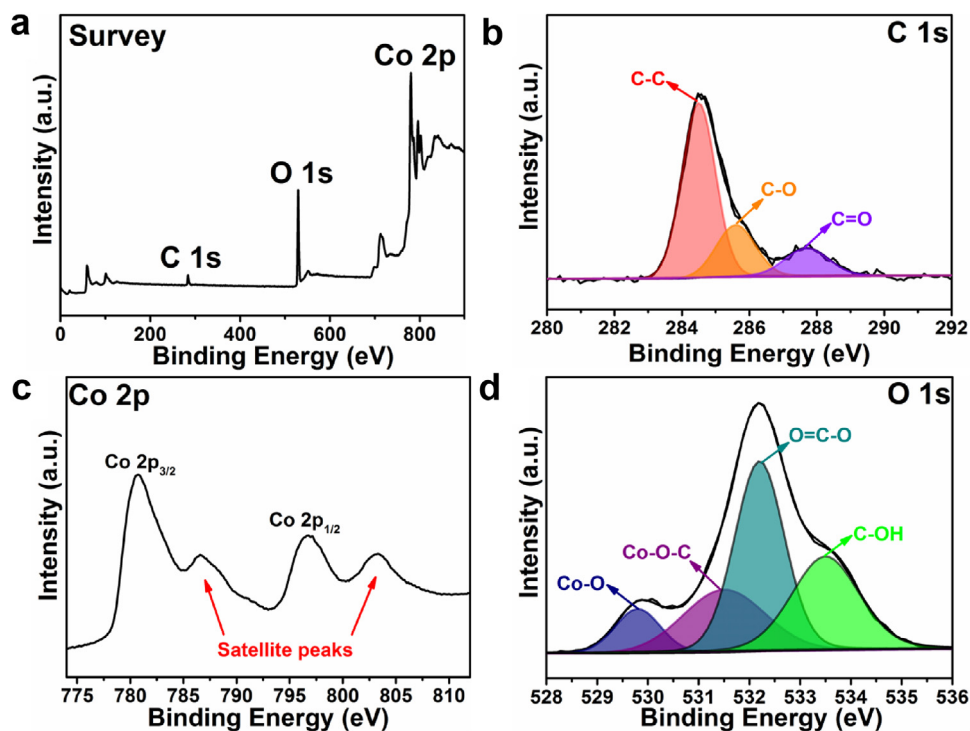
Fig. 4. XPS analysis of the 5% CDs-CoO composite: (a) survey XPS spectrum, (b) C 1s, (c) Co 2p and (d) O 1s high-resolution XPS spectra.
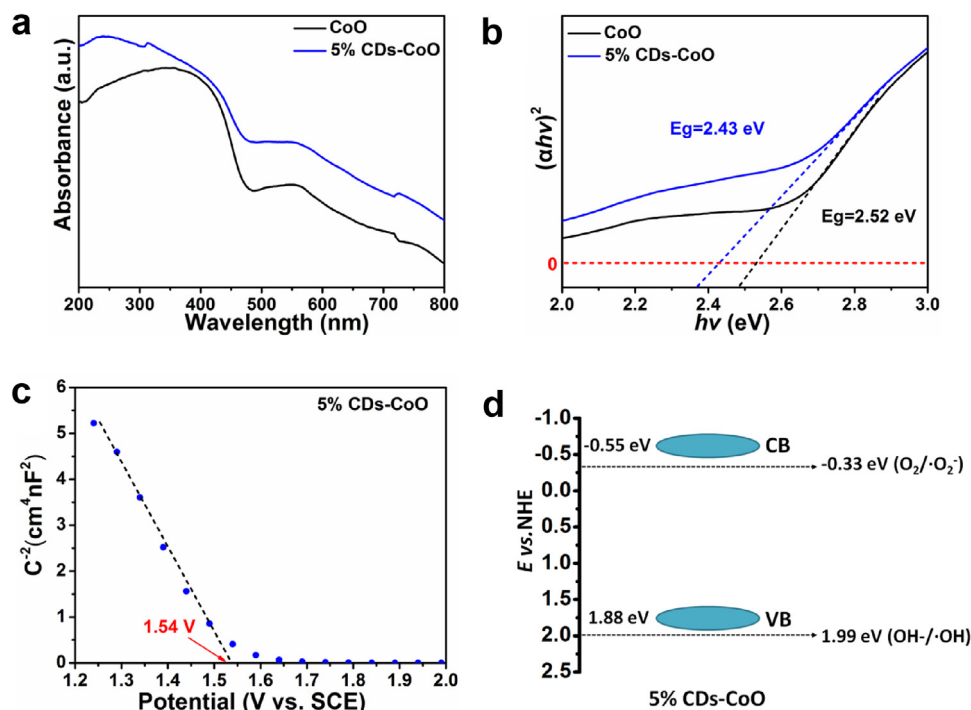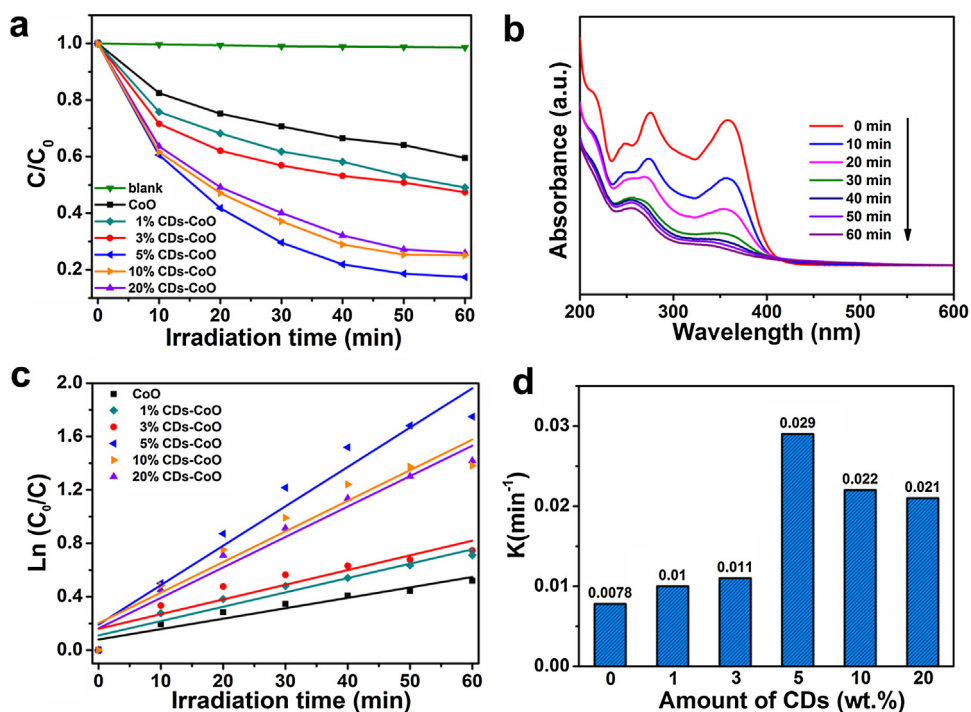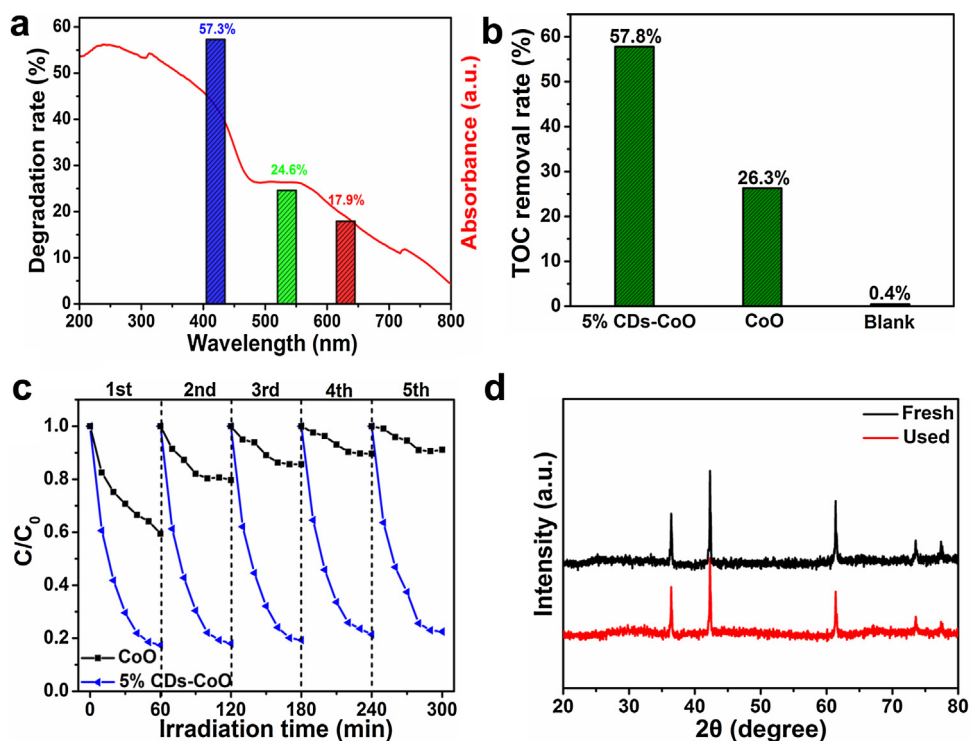

Fig. 5. (a) UV–vis diffuse reflectance spectra and (b) corresponding Plots of $(ahv)^2$ versus hv for the band gap energy over pristine CoO and 5% CDs-CoO composite. (c) Mott-Schottky plot and (d) energy band structure diagram of 5% CDs-CoO composite.

efficient separation and transfer of photo-induced electrons and holes in CDs-CoO composite system. In Fig. 8c, the photocurrent response is observed during on and off cycles of illumination. In comparison with CoO, 5% CDs-CoO exhibits higher photocurrent intensity, implying that the photo-induced charge carriers can be effectively transferred. EIS Nyquist plots of CoO and 5% CDs-CoO are shown in Fig. 8d. A smaller the arc radius of 5% CDs-CoO in compar-ison with CoO is obtained, demonstrating that the charge transfer occurrs more rapidly at the interface of CDs-CoO than CoO and thus promotes efficient separation of the photo-generated electron-hole pairs. Based on the results above, it draws the conclusion that the addition of CDs possesses positive effect on improving the photocurrent density and separation efficiency of photo-generated charge carriers in the CDs-CoO composite.

Fig. 6. (a) Photocatalytic activities of as-prepared photocatalysts for TC degradation under visible-light irradiation (λ > 420 nm). (b) Changes of the characteristic absorption of TC under different irradiation time by using 5% CDs-CoO as a photocatalyst. (c) The first-order-kinetic plots and (d) the corresponding rate constants of TC degradation over different photocatalysts.

Fig. 7. (a) The degradation rate of TC solution by 5% CDs-CoO photocatalyst as a function of wavelength of the incident light. A xenon lamp with band-pass filters of 420 nm, 530 nm and 630 nm wavelength was used as a light source. (b) TOC removal rate of TC (C_0 = 10 mg/L) over the CoO, 5% CDs-CoO and directly photolysis after 60 min visible light irradiation (λ > 420 nm). (c) Five recycling runs over pure CoO and 5% CDs-CoO photocatalysts in degradation of TC. (d) XRD patterns of before and after photocatalysis over 5% CDs-CoO heterojunction photocatalyst in degradation of TC.

It is important to determine the main active species in the photocatalytic reaction process to understand the photocatalytic mechanism. In this study, three sacrificial agents including iso-propanol (IPA), ethylene diamine tetraacetic acid disodium salt

(EDTA-2Na) and benzoquinone (BQ) were applied as •OH, h^+ and •O_2^- scavengers, respectively (Fig. 9a). It can be seen that with 1 mmol of IPA as a •OH scavenger added into the solution, the degradation rate of TC over 5% CDs-CoO sample is not obviously
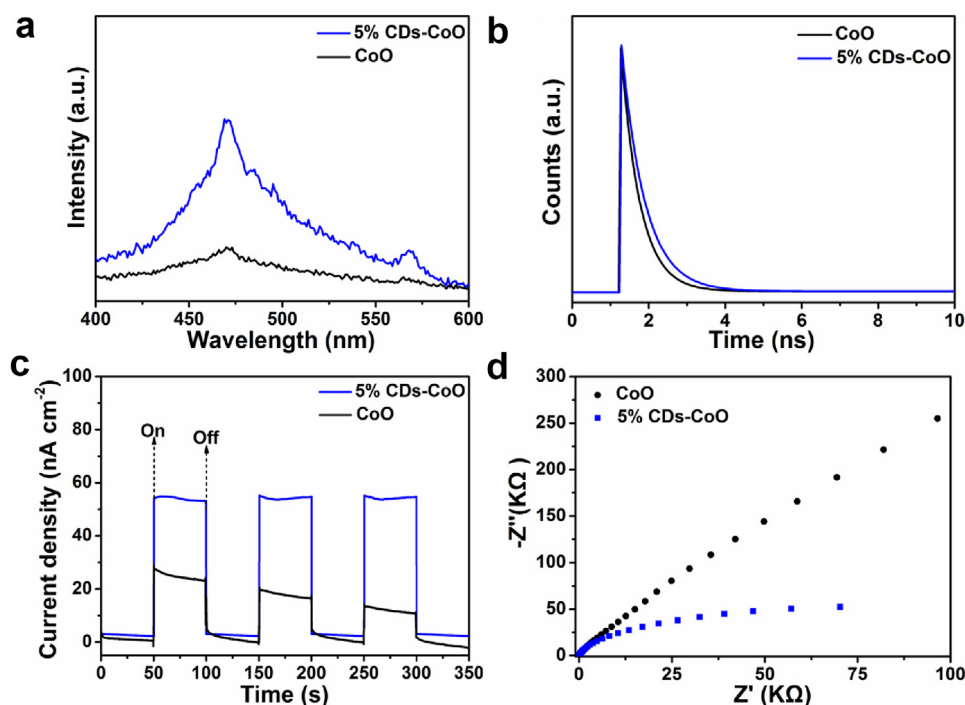
Fig. 8. (a) PL spectra, (b) Time-resolved fluorescence decay fitting curves, (c) Transient photocurrent responses and (d) EIS changes of CoO and 5% CDs-CoOs.
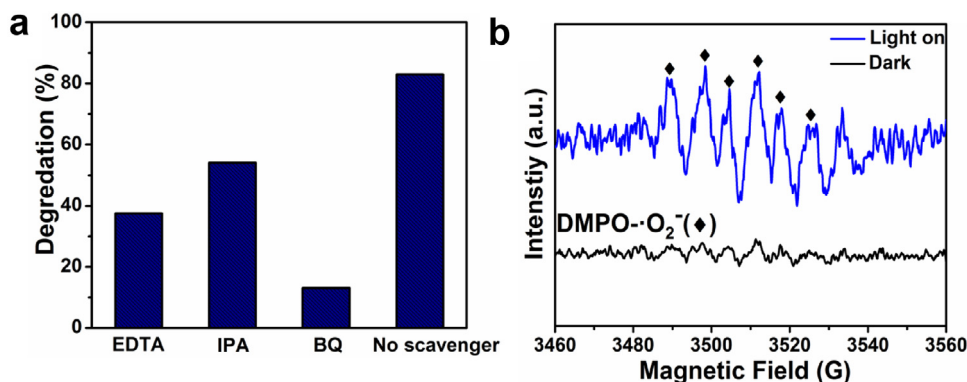

Fig. 9. (a) Trapping experiment of active species during the photocatalytic degradation of TC over 5% CDs-CoO photocatalyst under visible light irradiation. (b) DMPO spin-trapping ESR spectrum for 5% CDs-CoO in methanol dispersion for DMPO-$^\bullet O_2^-$.

affected, indicating that the $^\bullet$OH is not the main reactive specie. However, when enzoquinone (BQ) as $^\bullet O_2^-$ scavenger and EDTA-2Na (quencher of h^+) are applied, the photodegradation process could be restricted efficiently. The result of trapping experiment reveals that the $^\bullet O_2^-$ and h^+ take more important effects in photocatalysis process. Additionally, DMPO spin-trapping ESR spectrum was further used to verify $^\bullet O_2^-$ of CDs-CoO composite during the photodegradation process, and the results are shown in Fig. 9b. Obviously, when the light is on, the characteristic signals of the DMPO-$^\bullet O_2^-$ could be observed. Consequently, according to the free radicals trapping experiments and ESR analysis, we can conclude that the h^+ and $^\bullet O_2^-$ radicals are the main reactive species but not the $^\bullet$OH radicals, which is agreement with the theoretical energy band structure (Fig. 5d).

On the basis of experimental results above, the possible enhanced photocatalytic mechanism in CDs-CoO composite system has been proposed in Fig. 10. The electrons and holes of CoO can be separated efficiently under visible light irradiation, which the electrons are transferred to the CB, leaving the holes on the VB. Generally, these photo-generated electrons and holes would

quickly recombine and only a spot of charges could take part in the photocatalytic reaction. Significantly, after combining CDs with the (111) highly active facets of CoO octahedrons to form CDs-CoO composite, large numbers of the photo-generated electrons on the CB of CoO tend to transfer to the CDs, consequently, the electrons on the CDs readily combine with oxygen in the solution to form $^\bullet O_2^-$, which is a strong oxidizing agent to degrade TC, and the holes on the VB of CoO would directly oxidize the pollutants, resulting in efficient electron-hole pairs separation and thus an enhanced photocatalytic activity.

4. Conclusion

In summary, we have successfully designed CDs-CoO composite composed of CDs-loaded on the exposing (111) highly active facets of CoO octahedrons via one-step solvothermal method for the degradation of TC under the visible light irradiation. Results show that all the CDs-CoO composites present superior photocatalytic activity and remarkable photostability. This enhanced photocatalytic activity and outstanding stability in CDs-CoO com-
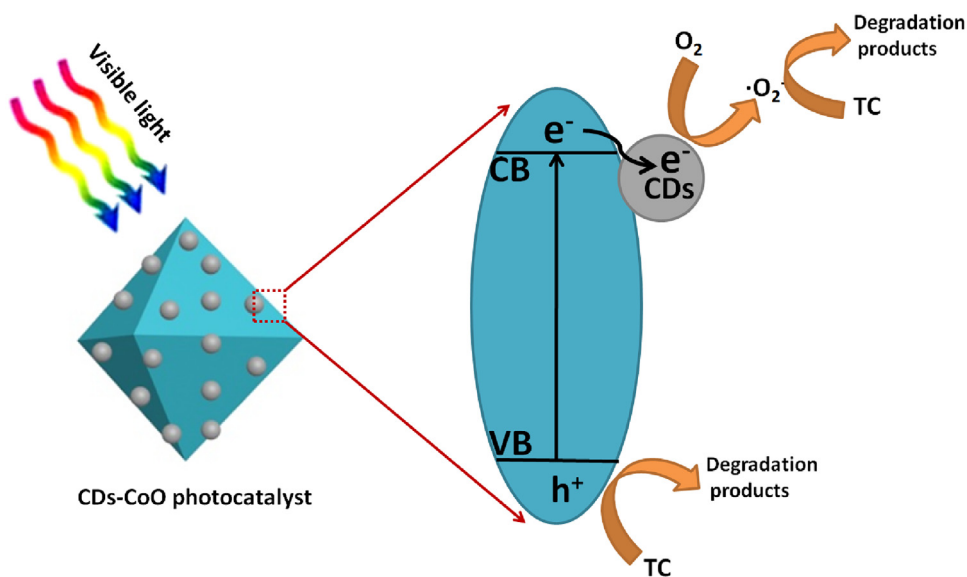
Fig. 10. Possible mechanism of the enhanced photocatalytic activity in the CDs-CoO composite system.

posites could be ascribed to several merits of CDs that not only improve charge separation efficiency but also strengthen the synergistic interaction between CDs and high-reactive (111) facets of CoO octahedrons. This work provides an efficient method to design highly-effective composite photocatalysts for the environmental remediation.

Acknowledgements

References

[1] C. Chen, W. Ma, J. Zhao, Chem. Soc. Rev. 39 (2010) 4206–4219.
[2] Y. Bi, S. Ouyang, N. Umezawa, J. Cao, J. Ye, J. Am. Chem. Soc. 133 (2011) 6490–6492.
[3] J. Jiang, K. Zhao, X.Y. Xiao, L.Z. Zhang, J. Am. Chem. Soc. 134 (2012) 4473–4476.
[4] K.B. Zhou, Y.D. Li, Angew. Chem. Int. Ed. 51 (2012) 602–613.
[5] D.Q. Zhang, S.L. Wang, J. Zhu, H.X. Li, Y.F. Lu, Appl. Catal. B: Environ. 123 (2012) 398–404.
[6] H. Zhao, W.Y. Yin, M.Y. Zhao, Y.Z. Song, H.Q. Yang, Appl. Catal. B: Environ. 130 (2013) 178–186.
[7] H.G. Yang, G. Liu, S.Z. Qiao, C.H. Sun, Y.G. Jin, S.C. Smith, J. Zou, H.M. Cheng, G.Q. Lu, J. Am. Chem. Soc. 131 (2009) 4078–4083.
[8] G.C. Xi, J.H. Ye, Chem. Commun. 46 (2010) 1893–1895.
[9] Y. Zhou, Z.P. Tian, Z.Y. Zhao, Q. Liu, J.H. Kou, X.Y. Chen, J. Gao, S.C. Yan, Z.G. Zou, ACS Appl. Mater. Interface 3 (2011) 3594–3601.
[10] Z.K. Zheng, B.B. Huang, Z.Y. Wang, M. Guo, X.Y. Qin, X.Y. Zhang, P. Wang, Y. Dai, J. Phys. Chem. C 113 (2009) 14448–14453.
[11] J. Wollenstein, M. Burgmair, G. Plescher, T. Sulima, J. Hildenbrand, H. Bottner, I. Eisele, Sens. Actuators B Chem. 93 (2003) 442–448.
[12] B. Liu, L. Ma, L.C. Ning, C.J. Zhang, G.P. Han, C.J. Pei, H. Zhao, S.Z. Liu, H.Q. Yang, ACS Appl. Mater. Interface 7 (2015) 6109–6117.
[13] A. Navrotsky, C. Ma, K. Lilova, N. Birkner, Science 330 (2010) 199–201.
[14] N. Fontaina-Troitino, S. Liebana-Vinas, B. Rodriguez-Gonzalez, Z.A. Li, M. Spasova, M. Farle, V. Salgueirino, Nano Lett. 14 (2014) 640–647.
[15] A. Navrotsky, MRS Bull. 41 (2016) 139–145.
[16] N. Birkner, A. Navrotsky, Proc. Natl. Acad. Sci. 111 (2014) 6209–6214.
[17] Z.A. Li, N. Fontaina-Troitino, A. Kovacs, S. Liebana-Vinas, M. Spasova, R.E. Dunin-Borkowski, M. Muller, D. Doennig, R. Pentcheva, M. Farle, V. Salgueirino, Sci. Rep. 5 (2015) 7997.
[18] R. Liu, H. Huang, H. Li, Y. Liu, J. Zhong, Y. Li, S. Zhang, Z. Kang, ACS Catal. 4 (2014) 328–336.
[19] H. Li, M. Yang, J. Liu, Y. Zhang, Y. Yang, H. Huang, Y. Liu, Z. Kang, Nanoscale 7 (2015) 12068–12075.
[20] H. Li, W. Kong, J. Liu, N. Liu, H. Huang, Y. Liu, Z. Kang, Carbon 91 (2015) 66–75.
[21] X. Zhang, F. Wang, H. Huang, H. Li, X. Han, Y. Liu, Z. Kang, Nanoscale 5 (2013) 2274–2278.
[22] W.L. Shi, F. Guo, M.M. Han, S.L. Yuan, W.S. Guan, H. Li, H. Huang, Y. Liu, Z.H. Kang, J. Mater. Chem. B 5 (2017) 3293–3299.
[23] H. Ming, Z. Ma, Y. Liu, K. Pan, H. Yu, F. Wang, Z. Kang, Dalton Trans. 41 (2012) 9526–9531.
[24] F.L. Wang, P. Chen, Y.P. Feng, Z.J. Xie, Y. Liu, Y.H. Su, Q.X. Zhang, Y.F. Wang, K. Yao, W.Y. Lv, G.G. Liu, Appl. Catal. B: Environ. 207 (2017) 103–113.
[25] J. Liu, Y. Liu, N. Liu, Y. Han, X. Zhang, H. Huang, Y. Lifshitz, S.T. Lee, J. Zhong, Z. Kang, Science 347 (2015) 970–974.
[26] H. Zhang, H. Huang, H. Ming, H. Li, L. Zhang, Y. Liu, Z. Kang, J. Mater. Chem. 22 (2012) 10501.
[27] P. Chen, F. Wang, Z.F. Chen, Q. Zhang, Y. Su, L. Shen, K. Yao, Y. Liu, Z. Cai, W. Lv, G. Liu, Appl. Catal. B: Environ. 204 (2017) 250–259.
[28] T.F. Yeh, C.Y. Teng, S.J. Chen, H.S. Teng, Adv. Mater. 26 (2014) 3297.
[29] X.Q. Wu, J. Zhao, S.J. Guo, L.P. Wang, W.L. Shi, H. Huang, Y. Liu, Z.H. Kang, Nanoscale 8 (2016) 17314–17321.
[30] H.M. Yang, J. Ouyang, A.D. Tang, J. Phys. Chem. B 111 (2007) 8006–8013.
[31] G.A.M. Hutton, B. Reuillard, B.C.M. Martindale, C.A. Caputo, C.W.J. Lockwood, J.N. Butt, E. Reisner, J. Am. Chem. Soc. 138 (2016) 16722–16730.
[32] A.V. Ravindra, B.C. Behera, P. Padhan, J. Nanosci. Nanotechnol. 14 (2014) 5591–5595.
[33] J. Lu, J.X. Yang, J.Z. Wang, A.L. Lim, S. Wang, K.P. Loh, ACS Nano 3 (2009) 2367–2375.
[34] Y. Yang, N. Liu, S. Qiao, R. Liu, H. Huang, Y. Liu, New J. Chem. 39 (2015) 2815–2821.
[35] L. Liao, Q. Zhang, Z. Su, Z. Zhao, Y. Wang, Y. Li, X. Lu, D. Wei, G. Feng, Q. Yu, X. Cai, J. Zhao, Z. Ren, H. Fang, F. Robles-Hernandez, S. Baldelli, J. Bao, Nat. Nanotechnol. 9 (2014) 69–73.
[36] Y. Sun, Y. Zhou, C. Zhu, L. Hu, M. Han, A. Wang, H. Huang, Y. Liu, Z. Kang, Nanoscale 9 (2017) 5467–5474.
[37] Q.M. Yu, J.X. Xu, C.Y. Wan, C.X. Wu, L.H. Guan, J. Mater. Chem. A 3 (2015) 16419–16423.
[38] Q. Qi, Y. Chen, L. Wang, D. Zeng, D.L. Peng, Nanotechnol 27 (2016) 455602.
[39] D. Barreca, A. Gasparotto, O.I. Lebedev, C. Maccato, A. Pozza, E. Tondello, S. Turner, G. Van Tendeloo, CrystEngComm 12 (2010) 2185–2197.
[40] Y. Matsumoto, Energy positions of oxide semiconductors and photocatalysis with iron complex oxides, J. Solid State Chem. 126 (1996) 227–234.
[41] B.A. Pinaud, Z.B. Chen, D.N. Abram, T.F. Jaramillo, J. Phys. Chem. C 115 (2011) 11830–11838.
[42] W. Wang, Y. Ni, Z. Xu, J. Alloy Compd. 622 (2015) 303–308.
[43] H. Song, L. Zhu, Y. Li, Z. Lou, M. Xiao, Z. Ye, J. Mater. Chem. A 3 (2015) 8353–8360.
[44] X. Zhang, T. Peng, L. Yu, R. Li, Q. Li, Z. Li, ACS Catal. 5 (2015) 504–510.
[45] J.B. Chen, H.N. Che, K. Huang, C.B. Liu, W.D. Shi, Appl. Catal. B: Environ. 192 (2016) 134–144.